Electronic Supplementary Material (ESI) for Materials Advances.

Supplementary Information

Detection of specific antibodies against SARS-CoV-2 spike protein via ultra-sensitive bio-functionalized carbon-nitride reduced graphene oxide electrochemical immunosensing platform in real samples

Mohd. Abubakar Sadique[1,2], Shalu Yadav[1,2], Pushpesh Ranjan[1,2], Raghuraj Singh Chouhan[3]*, Ivan Jerman[4], Ashok Kumar[5], Saurabh Saigal[5], Sagar Khadanga[5], Raju Khan[1,2,*] and Avanish K. Srivastava[1]

[1]CSIR–Advanced Materials and Processes Research Institute (AMPRI), Hoshangabad Road, Bhopal - 462026, India
[2]Academy of Scientific and Innovative Research (AcSIR), Ghaziabad - 201002, India
[3]Jožef Stefan Institute, Jamova Cesta-39, Ljubljana - 1000, Slovenia
[4]National Institute of Chemistry, Hajdrihova 19, Ljubljana - 1000, Slovenia
[5]All India Institute of Medical Sciences (AIIMS), Bhopal - 462020, India

*Corresponding author Email:
Raghuraj Singh Chouhan (raghuraj.singh@ijs.si)
Raju Khan (khan.raju@gmail.com)

Experimental Section

Synthesis of Graphene oxide

Tour's method was used to synthesize graphene oxide (GO).[1] To elaborate, H_2SO_4 and H_3PO_4 were mixed in a 9:1 ratio. The above solution was kept in an ice bath keeping the temperature < 15 ^oC. To the above solution, a pre-mixed mixture of graphite powder and $KMnO_4$ in a 1:6 ratio was added gradually. The solution turned greenish-black, and the temperature was maintained below 20 ^oC to avoid any sudden bursts. The solution was kept at constant stirring for 1 h for the complete mixing into the solvent. Further, the temperature was raised to 50 ^oC and maintained by an oil bath for 24 h at constant stirring. After completion of the reaction, the mixture was kept cooling till an ambient temperature (27 ^oC). After oxidation, the color of the solution changed to brownish-black. To the above solution, milli-Q water and H_2O_2 were added to stop the reaction. The color of the solution changed to yellowish-brown indicating the formation of GO. The GO suspension was settled down and the sediments were washed thrice with each HCl, milli-Q water, and ethanol until the pH of the solution became neutral. The solution was collected through centrifugation after the removal of unwanted materials. The obtained solution was dried in a hot air oven at 60 ^oC, weighed, and stored for experimental use.

Cleaning of Glassy carbon electrodes

The working electrodes (Glassy carbon electrodes (GCEs)) were cleaned by a standard cleaning procedure. Firstly, The GCEs were sonicated in ethanol. Further, the electrodes were polished with alumina slurry of 0.3 and 0.05 μm alternatively for 10 min. At last, the electrodes were sonicated in milli-Q water to remove alumina and other impurities. The electrodes were air-dried and kept in a desiccator before modification with nanomaterials.

Characterization

Atomic Force Microscopy

To evaluate the surface uniformity and thickness of C_3N_4 nanosheets, atomic force microscopy (AFM) was carried out. The optical image of the surface roughness is seen in **Fig. S1A** at the scale of 1 µm. The height profile of the nanosheets in **Fig. S1B** suggests the film thickness be around 2-3 nm. Since the thickness of the monolayer of C_3N_4 is about 0.3-0.4 nm, the synthesized C_3N_4 would consist of 6-8 layers.[2]

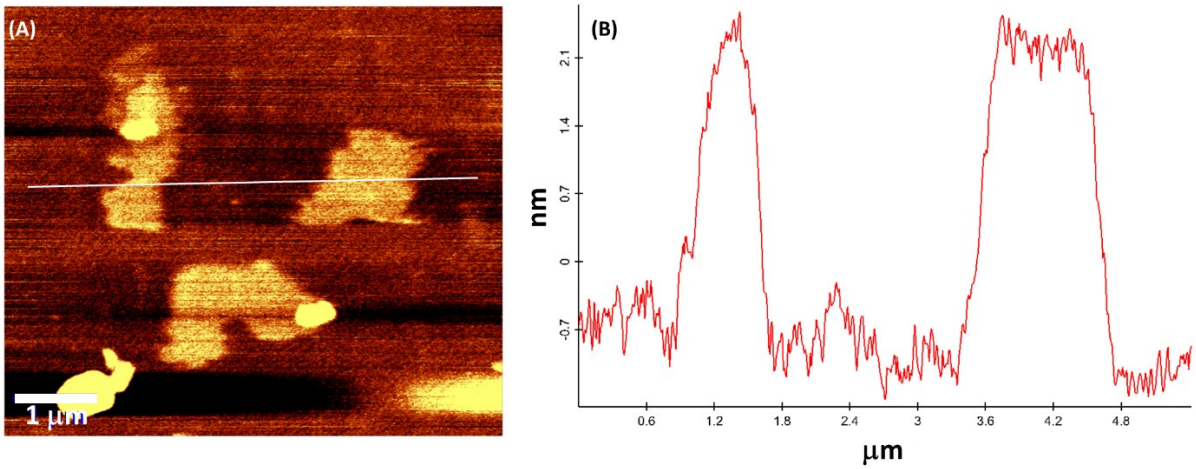

Fig. S1. (A) AFM analysis at 1 µm scale and **(B)** the height profile of C_3N_4 nanosheets.

X-ray photoelectron spectroscopy (XPS)

The base material C_3N_4 has been characterized by XPS for analysis of the binding energy of the carbon and nitrogen atoms involved in the formation of graphitic C_3N_4 nanosheets. In the XPS spectra (**Fig. S2A**) concerning the binding energy of N 1s, the obtained peaks at 389.72, 399.72, and 400.97 eV correspond to sp^2 bonded N atom in the triazine rings, amino-functional group (C–N–H), and tertiary nitrogen N atom in N–$(C)_3$ respectively. Moreover, in the XPS spectra (**Fig. S2B**) concerning the binding energy of C 1s, two peaks around 284.77 and 288.15 eV correspond to sp^2 C–C bonds and sp^2 C in an N-containing aromatic ring, respectively.[3] The XPS spectra suggest a C and N intermixed backbone structure of C_3N_4 nanosheets. In **Fig. S2C**, survey spectra show the distinctive presence of N 1s peak around 400 eV and C 1s peak around 280 eV. The absence of the O 1s peak suggests that there are no oxygen-containing impurities in the compound and the synthesized C_3N_4 nanosheets are free from any surface-adsorbed oxygen as well.

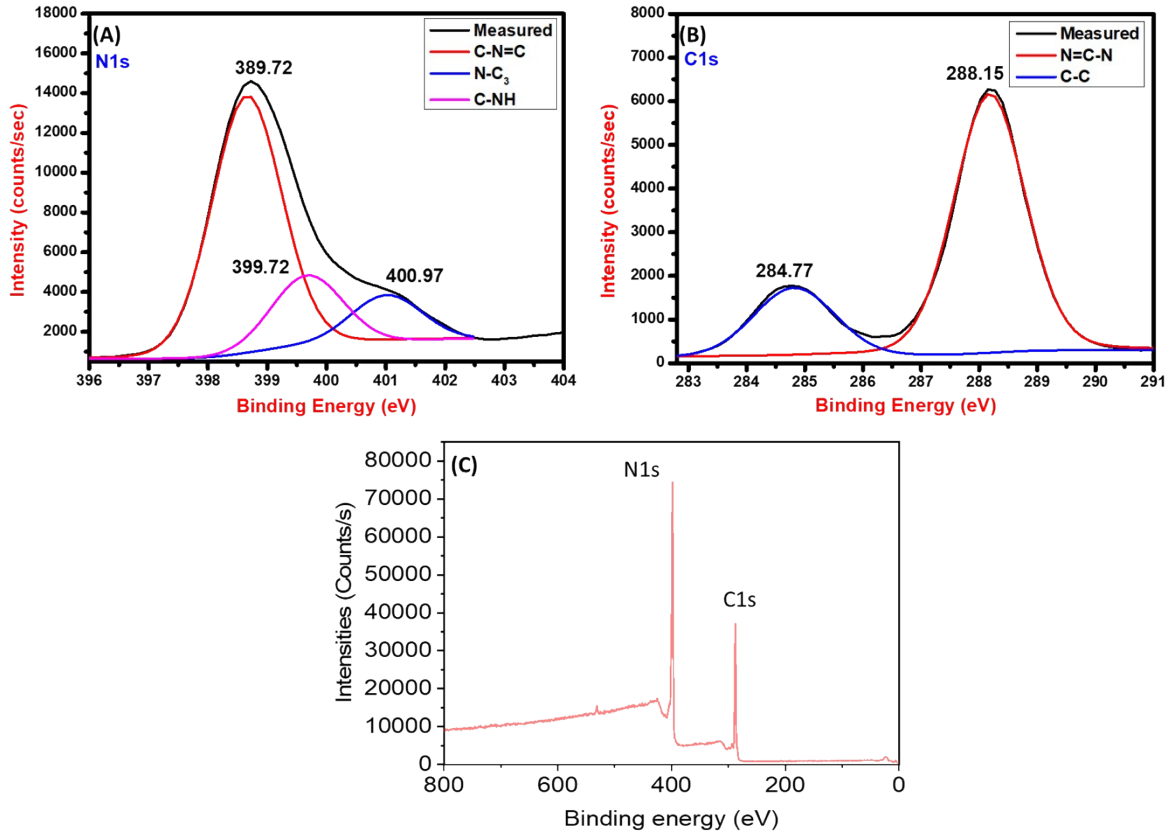

Fig. S2. XPS analysis of **(A)** N 1s region, **(B)** C 1s region of C_3N_4 nanosheets, and **(C)** Survey spectra of C_3N_4 nanosheets.

Morphological analysis of C_3N_4

The SEM image of the C_3N_4 nanosheets shown in **Fig. S3** depicts the flaky nature of C_3N_4 nanosheets. The synthesized C_3N_4 nanosheets have the morphology of sheets in nanoscale dimensions and dense agglomeration when seen at the 2 μm magnification. The morphological analysis suggests that C_3N_4 nanosheets have a good capability to be utilized as a two-dimensional nanomaterial for electrode modification.

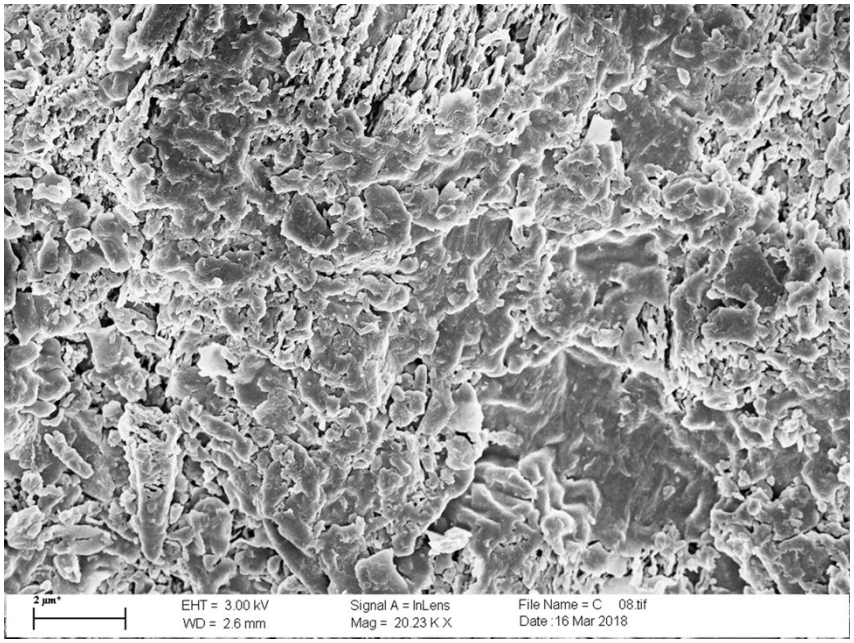

Fig. S3. SEM image of C_3N_4 nanosheets at 2 μm magnification.

Electrochemical studies

Randles Circuit Fit

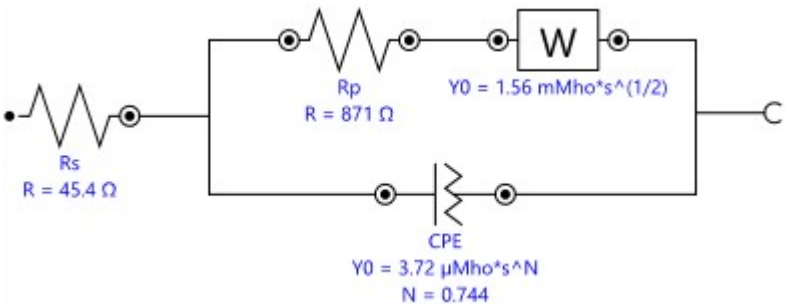

Fig. S4: Randles Fitted Circuit for C_3N_4.[4]

Scan Rate studies

The electrochemical reversibility of the synthesized bio-functionalized C_3N_4/RGO nanocomposite and fabricated immunosensor was analyzed by scan rate studies. The CV technique was used where variation in scan rate was done from 10 to 100 mV s^{-1} in PBS (pH 7.4) for both bio-functionalized C_3N_4/RGO nanocomposite and immunosensor respectively as shown in **Fig. S5(A, B)**. The anodic and cathodic peak currents increase linearly with an increase in scan rates, corresponding shifts are observed in anodic and cathodic peak potentials as well.

A linear relationship between anodic (I_{p_A}) and cathodic peak currents (I_{p_C}) vs. square root of scan rate ($\nu^{1/2}$) for the bio-functionalized C_3N_4/RGO nanocomposite as well as immunosensor was studied by their respective regression curves.

$$I_{p_A\ C_3N_4/RGO/Chi}\ (\mu A) = +\ 7.05 \times \nu^{1/2} + 6.57, \quad R^2 = 0.996 \qquad \text{(S1)}$$

$$I_{p_C\ C_3N_4/RGO/Chi}\ (\mu A) = -\ 8.15 \times \nu^{1/2} - 6.72, \quad R^2 = 0.999 \qquad \text{(S2)}$$

$$I_{p_A\ Immunosensor}\ (\mu A) = +\ 6.22 \times \nu^{1/2} + 9.25, \quad R^2 = 0.998 \qquad \text{(S3)}$$

$$I_{p_C\ Immunosensor}\ (\mu A) = -\ 7.37 \times \nu^{1/2} - 4.65, \quad R^2 = 0.987 \qquad \text{(S4)}$$

As seen from the regression curves from the insets of **Fig. S5(A, B)**, the reaction kinetics follow a diffusion-controlled transfer of electrons.[5] Moreover, the high value of the correlation coefficient (R^2) suggests the quasi-reversible nature of the modified electrodes. The corresponding equations show excellent linearity.

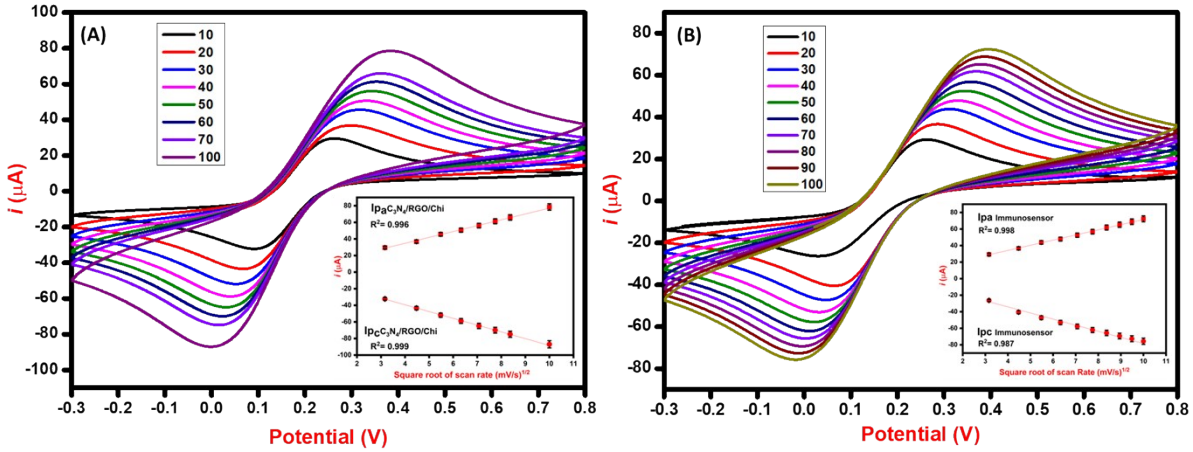

Fig. S5. Scan rate study of **(A)** bio-functionalized C_3N_4/RGO nanocomposite, and **(B)** fabricated immunosensor in 0.1 M PBS containing 0.1 M KCl and 5 mM ferri/ferrocyanide redox solution, pH=7.4.

Table S1: A comparative analysis of C_3N_4-based biosensors related to the SARS-CoV-2 virus.

S.No.	Sensing platform	Target Analyte	Detection Technique	Sample	Limit of Detection	Linear Range	Reference
1.	Aptamer/chitosan/CdS QDs-gC_3N_4/ITO	SARS-CoV-2 RBD	PEC	Human saliva	0.12 nM	0.5-32 nM	[6]
2.	g-C_3N_4 nanosheets and Ru–SiO_2@folic acid nanomaterials	SARS-CoV-2 virus (RdRp gene)	ECL	Human throat swab	0.18 fM	1 fM to 10 nM	[7]
3.	(Bi_2WO_6/Bi_2S_3) and (g-C_3N_4/Au/WO_3)	SARS-CoV-2 N-protein	DPV	Saliva	3 fg mL^{-1}	0.01 to 1 pg mL^{-1}	[8]
4.	PdNPs/g–C_3N_4–S /ST/ FTO	SARS-CoV-2 spike	PEC	Artificial saliva	1 fg mL^{-1}	1 fg mL^{-1} to 1000 pg mL^{-1}	[9]
5.	C_3N_4-Au NPs	SARS-CoV-2 protein		ssDNA saliva samples	2.2 fmol L^{-1}	1 to 10000 fmol L^{-1}	[10]
6.	bio-functionalized C_3N_4/RGO nanocomposite	SARS-CoV-2 antibodies	DPV	Serum	1.73 ag mL^{-1}	100 ag mL^{-1} to 100 ng mL^{-1}	**This Work**

*PEC= Photoelectrochemical; ECL= Electrochemiluminescence; DPV= Differential pulse Voltammetry

References

1 D. C. Marcano, D. v Kosynkin, J. M. Berlin, A. Sinitskii, Z. Sun, A. Slesarev, L. B. Alemany, W. Lu and J. M. Tour, *American Chemical Society*.

2 S. Zhang, N. T. Hang, Z. Zhang, H. Yue and W. Yang, *Nanomaterials*, 2017, **7**, 1–11.

3 R. S. Chouhan, G. Žitko, V. Fajon, I. Živković, M. Pavlin, S. Berisha, I. Jerman, A. Vesel and M. Horvat, *Sensors (Switzerland)*, , DOI:10.3390/s19153432.

4 A. L. Lorenzen, A. M. dos Santos, L. P. dos Santos, L. da Silva Pinto, F. R. Conceição and F. Wolfart, *Electrochim Acta*, 2022, **404**, 139757.

5 R. Devi, S. Gogoi, H. S. Dutta, M. Bordoloi, S. K. Sanghi and R. Khan, *Nanoscale Adv*, 2020, **2**, 239–248.

6 M. Amouzadeh Tabrizi, L. Nazari and P. Acedo, *Sens Actuators B Chem*, 2021, **345**, 130377.

7 T. Yin, Y. Ye, W. Dong and G. Jie, *Biosens Bioelectron*, 2022, **215**, 114580.

8 C. Karaman, B. B. Yola, O. Karaman, N. Atar, İ. Polat and M. L. Yola, *Mikrochim Acta*, 2021, **188**, 425.

9 C. N. Botelho, S. S. Falcão, R.-E. P. Soares, S. R. Pereira, A. S. de Menezes, L. T. Kubota, F. S. Damos and R. C. S. Luz, *Biosens Bioelectron X*, 2022, **11**, 100167.

10 L. G. da S. Catunda, T. Martimiano do Prado, T. R. de Oliveira, D. J. Almeida dos Santos, N. O. Gomes, D. S. Correa, R. C. Faria and S. A. S. Machado, *Electrochim Acta*, 2023, **451**, 142271.